2025-01-8173 Published 01 Apr 2025

Impact of Thermal and Electrical Dissimilarities on Battery Module Aging

Andre Swarts, Swapnil S. Salvi, and Daniel Juarez Robles Southwest Research Institute

Citation: Swarts, A., Salvi, S.S., and Juarez Robles, D., "Impact of Thermal and Electrical Dissimilarities on Battery Module Aging," SAE Technical Paper 2025-01-8173, 2025, doi:10.4271/2025-01-8173.

Received: 31 Oct 2024 Revised: 20 Jan 2025 Accepted: 20 Jan 2025

Abstract

Battery cell aging and loss of capacity are some of the many challenges facing the widespread implementation of electrification in mobility. One of the factors contributing to cell aging is the dissimilarities of individual cells connected in a module. This paper reports the results of several aging experiments using a mini-module consisting of seven 5 Ah 21700 lithium-ion battery cells connected in parallel. The aging cycle comprised a constant current-constant voltage charge cycle at a 0.7C C-rate, followed by a 0.2C constant current discharge, spanning the useful voltage range from minimum to maximum according to the cell manufacturer. Charge and discharge events were separated by one-hour rest periods and were repeated for four weeks. Weekly reference performance tests were executed to measure static capacity, pulse power capability and resistance at different states of charge. All diagnostics were normalized with respect to their starting numbers to achieve a percentage change over time. Both electrical and thermal dissimilarities were considered by initial cell selection or adjusting the thermal boundary conditions, respectively. The latter was achieved by contrasting air cooling with direct liquid immersion cooling which prevented temperature spikes and ensured more uniform temperature distribution between the cells. For well-clustered cells, the use of immersion cooling reduced the capacity fade noticeably when compared to air cooling. However, when cells are not well clustered, the impact of electrical dissimilarities overshadowed the thermal benefits. Poor cell clustering resulted in a lower discharge resistance increase which itself reflected as smaller changes of the pulse power fade. The results highlighted the importance of cell selection and clustering during research and when building packs for final application and reinforced the benefits of good thermal management. The work did not fully explore the benefits of immersion cooling due to the moderate C-rates used.

Introduction

Thermal management is a critical aspect of maintaining the performance and safety of lithium-ion batteries (LIBs), especially under high discharge rates. Various cooling strategies have been explored to mitigate temperature rise and enhance heat dissipation. Air-based cooling systems, though widely used, have limitations in achieving uniform temperature distribution across cells, particularly during fast charging or discharging [1,2]. Indirect liquid cooling, in contrast, offers significantly better thermal performance, with studies showing improved cooling efficiency through liquid plates and coolant channels [3,4]. Furthermore, the application of phase change materials (PCMs) has been investigated to reduce temperature spikes by absorbing excess heat during operation [5,6].

Among advanced cooling techniques, direct liquid immersion cooling, where the battery cells are submerged directly in a dielectric fluid, has emerged as a promising approach due to its ability to maintain temperature uniformity while preventing thermal runaway [7,8]. By enabling direct contact between the coolant and battery surface, immersion cooling offers a higher heat transfer coefficient compared to conventional methods. Experimental studies have demonstrated substantial reductions in cell temperature at high discharge currents using immersion cooling [9,10]. Additionally, immersion cooling can reduce the risk of localized hot spots, which are common in air or indirect liquid cooling systems, improving both the safety and longevity of the battery pack [7]. Recent experimental research has focused on optimizing the performance of immersion cooling systems through fluid selection and flow control. For example, Williams et al. (2024) investigated the use of Novec7000 in a two-phase cooling system, observing enhanced thermal performance in closely packed cells at elevated charge-discharge rates [11]. Similarly, Goa et al. explored the effectiveness of fish-shaped flow guides, demonstrating improved heat

dissipation and higher Nusselt numbers compared to traditional flow designs [12]. Further studies by Hemavathi et al. and Liu et al. reported superior cooling performance using ester oils and mineral oils, with significant reductions in peak cell temperatures [13,14]. In high-current applications, Li et al. and Wang et al. demonstrated the advantages of using two-phase SF33 cooling to maintain consistent cell temperatures under fast charging conditions, emphasizing the importance of phase change and fluid agitation [15,16]. Choi et al. extended these findings by incorporating metal foam structures into the cooling system, further enhancing heat transfer capabilities, particularly for prismatic cells [17].

However, despite these clear advantages, concerns remain about the effects of immersion cooling on the electrochemical performance of battery cells, particularly in modules where electrical dissimilarity between cells can emerge and affect the performance of immersion cooled batteries. Salvi et al. [18] observed that capacity fade in immersion-cooled cells was more pronounced than in air-cooled cells. To investigate this phenomenon, a detailed analysis was conducted, testing several hypotheses through experimental measurements, and validating them with theoretical modeling and simulations to identify underlying factors contributing to this behavior. After rigorously testing these hypotheses, the exact cause of the increased capacity fade using immersion cooling remained undetermined.

In addition to thermal management, electrical dissimilarities between individual cells within a battery pack present a significant challenge to achieving optimal pack performance. Even slight variations in the production process or operational conditions can result in inconsistencies between cells, which tend to worsen over time [19]. These inconsistencies manifest as differences in state of charge (SOC), internal resistance, and capacity, which ultimately affect the overall performance and lifetime of the pack [20]. A pack's performance is constrained by its weakest cell, as the cell with the lowest capacity will determine the operational limits of the entire system [21]. To mitigate these issues, cell balancing techniques are employed to equalize the SOC and capacity across all cells, minimizing the effects of electrical dissimilarities. Overcharging and external short circuits are two common conditions that exacerbate these imbalances, leading to accelerated aging and increased internal resistance due to damage to the electrode materials and the growth of the solid electrolyte interphase (SEI) layer [22]. Clustering methods, commonly used in data-driven applications, have also been adapted to manage the performance inconsistencies in electric vehicle battery packs, offering a computational approach to optimize battery management systems [23].

In parallel-connected battery systems, electrical dissimilarities—such as variations in internal resistance or state of charge—result in uneven current distribution among cells. This imbalance can undermine the effectiveness of immersion cooling, as cells with higher resistance tend to generate more heat, worsening temperature disparities within the module. Consequently, some cells may undergo greater thermal stress, leading to accelerated degradation [18]. Preemptively clustering cells with similar electrical properties is crucial to prevent these dissimilarities from impacting overall module performance. While immersion cooling offers better temperature control than air cooling, it requires careful management of electrical imbalances to avoid performance degradation and safety risks. Employing modern clustering techniques is therefore key to optimizing immersion cooling in parallel-connected battery modules.

To investigate the relative contribution of thermal and electrical dissimilarities, the current study completed a series of aging experiments with different approaches to cell selection and clustering as well as thermal boundary conditions. Five separate tests were performed: Two tests using air (A1 and A2) cooling and four tests with direct immersion cooling with forced convection of three difference dielectric liquids (L1 through L4) with one fluid testing twice.

Experimental Setup

Cell Selection and Clustering

Commercially available LG Chem M50T 21700 cylindrical cells with lithium nickel manganese cobalt oxide (NMC) cathodes and graphitic anodes were selected for this study. The nominal cell capacity was 5.0 Ah with a nominal energy of 18.2 Wh. The manufacturer-specified cell resistance was 30 mΩ [24].

Cell clustering was done using cell features extracted from BOL (beginning of life) tests. The characteristic features were:

- Discharge static capacity in Ah.
- Time constant to achieve open circuit voltage (OCV) after completion of charging and after discharging the cell in seconds.
- Open circuit voltage at 100% SOC in Volt.
- Internal resistance (average of cell resistance at the end of charge and discharge) in Ohms.

A feature was dropped as a criterion for cell selection if its standard deviation was less than 0.5% of the mean. The Ward's D2 clustering method was applied to the chosen features. Clusters were progressively formed using the sum of squares as a distance between the centroids of the clusters being merged. The final set of clusters was organized in a hierarchical diagram called Dendrogram.

The magnitude of the difference between the features of the individual cells in a cluster were quantified by the Mahalanobis distance (MD). MD measured relative distance of a point from the overall mean for multivariate data. Since cell properties can be correlated, principal component axes are no longer orthogonal, thereby impeding a direct distance measurement. MD addressed this

FIGURE 1 Box-and-whisker plot of the MD for the six modules.

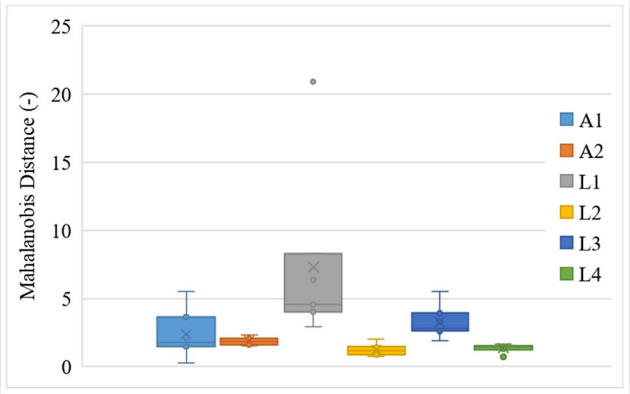

correlation by performing a rotation along the principal components of the data followed by a normalization.[25]

Cells for A1 and L1 modules construction were arbitrarily selected from a single batch of more than 100 cells, assuming minimal cell variation. The cells for A2 and L2 through L4 were intentionally selected to have well clustered characteristics. The consequence of this cell selection is shown in Figure 1 with box-and-whisker plots of the MD of the six cell clusters. The cells in L1 were particularly widely distributed and contained not only a wide distribution between the 1st and 3rd quartile but also a singular outlier at a value of more than 20, indicating at least one of the cells had electrical properties dissimilar to the rest of the cells. A1 and L3 had the next widest variability with tightest groupings seen for A2, L2 and L4. The data suggested that the arbitrary selection process may have introduced unintended variations in cell properties, despite the common batch origin. It should be noted that variability of the MD, and not the absolute values, were considered important for this paper.

The MD indicated the proximity of an individual cell to the mean of the population – the accuracy of the selection – whilst the variability of the MD of cells within a cluster indicated how close the cells were to each other – the precision of the selection.

Module Construction

As depicted in Figure 2, the cells were arranged in a 7PS1 (7 cells in parallel) configuration, where they were spot-welded to nickel metal bus bars, creating a flower-shaped cross-section. The spacing between cells was fixed at approximately 0.5 mm. The nominal module capacity was 35.0 Ah and a nominal energy of 91.0 Wh with the nominal module resistance at 4.28 mΩ. Two K-type thermocouples were attached to the surface of each cell using adhesive and tape for temperature monitoring: one close to the positive and one close to the negative terminal, with all thermocouples located in the gaps between the cells. The battery module was placed at the center of an enclosure, which was specifically designed to enable

FIGURE 2 Typical 7p1s module construction.

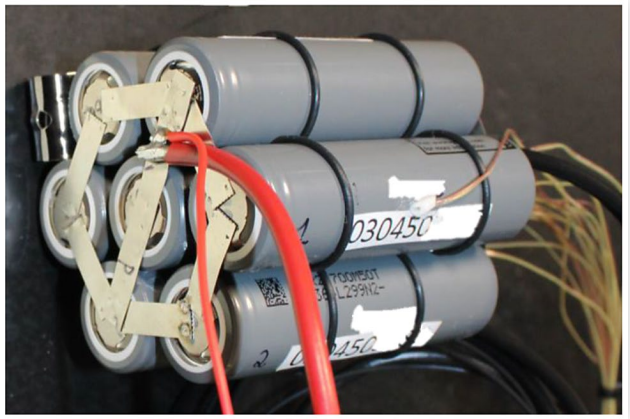

FIGURE 3 Schematic for test rig [18].

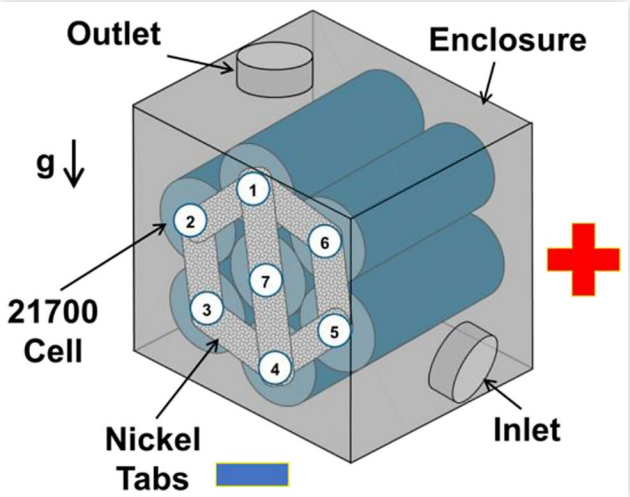

coolant flow around the cells. The enclosure provided approximately 5 mm of clearance between the cells and the enclosure walls, preventing direct electrical contact and allowing adequate space for thermocouples and other wiring necessary for connecting the module to the battery cycler. The enclosure was sized to achieve approximately 38% void space around the cells. Data from all thermocouples and the module voltage were captured via a National Instruments Compact-RIO data acquisition system.

Figure 3 illustrates the module location in the enclosure, with the flow inlet positioned on one side face and the outlet located on the top face. Both locations were fitted with thermocouples to monitor liquid temperatures at the inlet and outlet.

For the first air cooling test (A1), the inlet and outlet were open to the lab environment with no forced convection nor temperature control but with the enclosure lid in place. The repeat air cooling test (A2) was carried out inside a temperature controlled thermal chamber set at 25 °C, for better repeatability – keeping all other aspects as same as A1.

Immersion Cooling

For direct liquid immersion cooling tests, the enclosure was connected to a flow rig comprising of a pump, stacked-plate heat exchangers using chilled water as a cooling medium, a turbine flow meter, a bypass valve and a flow control valve. The latter was used to maintain the flow rate at 1.5 liters per minute based on the flow meter reading, with an additional control valve on the chilled water supply to keep the fluid inlet temperature to 25 °C. A lay-out of the flow rig is shown in Figure 4.

The nature and properties of the liquids used for immersion cooling were not relevant to this paper but all had appropriate heat transfer properties and sufficiently low electrical conductivity to prevent leakage.

Cycling

An SBT-2050 Power Cycler from PEC Corp. was employed to implement a fast charge current profile. The module underwent a five-day charge-discharge cycling period, followed by reference performance testing (RPT) on the sixth and seventh days. The charge-discharge cycling process included a one-hour rest period, followed by constant current constant voltage (CCCV) charging at a C-rate of 0.7 C - the maximum continuous current recommended by manufacturer for the cells - then another rest hour, and finally constant current (CC) discharge at 0.2 C, corresponding to the nominal current. The cells were cycled between voltage limits of 4.2 V and 2.5 V. To determine the cell capacity at the end of each cycle, the cells are charged at 0.3 C under CCCV conditions until 100% SOC was reached, and then discharged at 0.2 C under CC conditions to measure the static capacity in Ampere-hours. The C-rate, as commonly defined, refers to the inverse of the number of hours required to complete the charge/discharge process; higher C-rates signifying faster processes.

The RPT consisted of three key components, as depicted in Figure 5. First, the static capacity measurement assessed the cell's charge storage capability by

FIGURE 4 Typical flow rig layout [18].

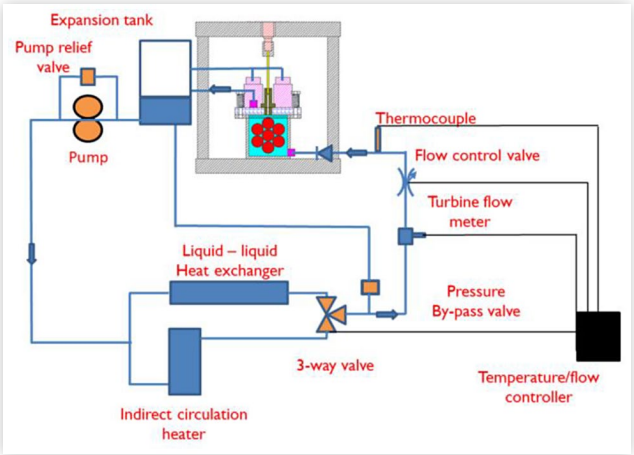

FIGURE 5 Reference performance test profile.

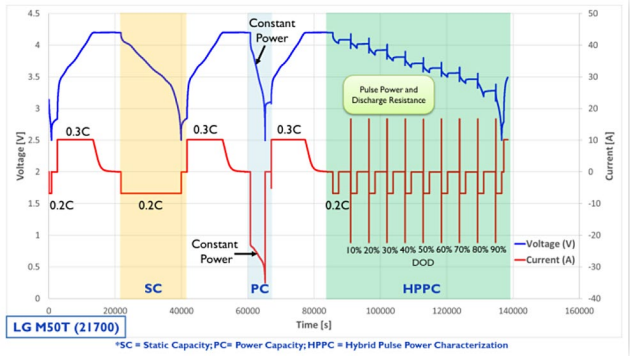

delivering a constant current over a specified period, typically at a slower discharge rate. Next, power capacity measurement evaluated the battery's ability to deliver high currents over short durations, representing its maximum power output under load. Lastly, the pulse power fade measurement focused on the cell's performance during repeated high-current pulses, simulating real-world scenarios with high power demands at different SOCs. The RPT methodology used in this study has been successfully applied in previous research to track cell performance degradation during cyclic aging.

Results

Thermal Conditions

A comparison of temperatures between air cooling and liquid immersion cooling revealed significant differences in thermal management effectiveness. As shown in Figure 6, during module cycling under air cooling conditions, extreme temperatures were observed, with peak values exceeding 50 °C during the charge phase of the cycle. The increase in cell voltage during the charge can be seen in the same plot. This resulted in a temperature increase of approximately 25 °C above the nominal test temperature. In contrast, the maximum temperature during immersion cooling testing was just over 27 °C, leading to a much smaller temperature increase of

FIGURE 6 Temperature comparisons for typical (a) air cooling (b) liquid immersion cooling

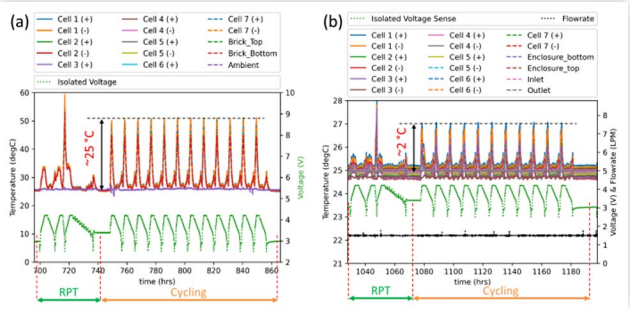

FIGURE 7 Cell temperature differences for a typical air cooling test.

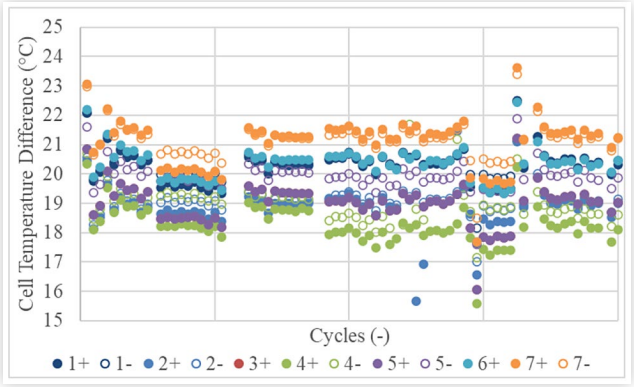

approximately 2 °C. A brief temperature spike can also be observed during the constant power step of the RPT but was not considered consequential for this analyses.

To better understand the temperature homogeneity, the temperature differences during charging was monitored for each of the 14 thermocouple locations. This temperature difference was calculated as the maximum during the charge minus the average during the rest period that followed the charge for each cell.

Figure 7 shows the cell temperature differences for a typical air test and revealed that the results varied depending on the location of the cell in the module. Thermocouples located near the positive terminal were indicated with filled symbols whilst those near the negative had open symbols. For the duration of the test, cell 7 at the center of the module, experienced the highest temperature differences with cell 4 at the bottom of the module consistently the coolest. The temperature results were also much more varied since the module temperature was affected by the laboratory ambient conditions.

Similar typical results for liquid immersion cooling are shown in Figure 8. Smaller differences within a cell were seen close to the flow inlet (cells 4 and 5) with larger differences for the cells at the top and the center of the module (cells 1 and 7 respectively). Unlike for air cooling, the center cell 7 did not have the highest temperature difference, suggesting the ability of the immersion cooling to affect heat transfer at the center of the module. The immersed test additionally exhibited a consistent upward trend in temperature differences as the test progressed, increasing by approximately 0.5 °C. A similar trend in the air cooling test may have been obscured by the overall temperature variability.

The overall test temperature differences for individual cells revealed not only the aforementioned cell-to-cell variations but also test-to-test variability. As seen in Figure 9, for a selected subset of the tests, there was very clear separation between air and liquid cooled tests with the former showing differences of greater than 20 °C and the latter less than 2.5 °C. It should be noted that these differences included the temporal changes seen above, such that the maximum temperature difference was typically at the end of the test whereas the minimum was at the

FIGURE 8 Cell temperature differences for a typical liquid immersion cooling test.

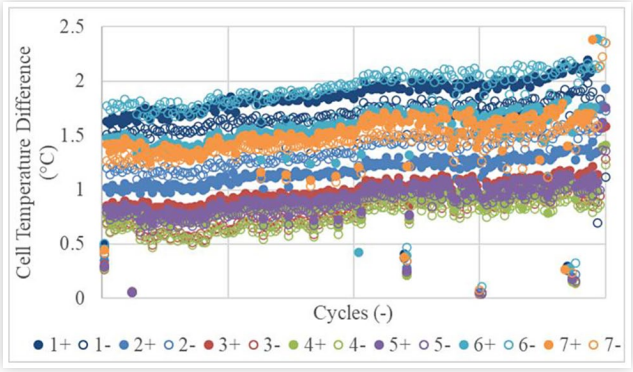

FIGURE 9 Overall test temperature differences for individual cells.

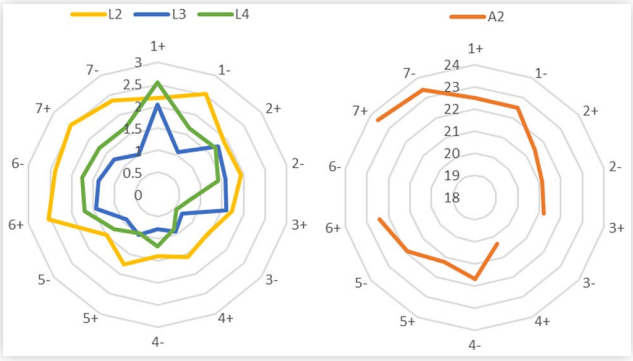

start. The lowest cell temperature differences were again consistently closest to the flow inlet and at the bottom of the module in the location of cells 3 and 4, regardless of the thermal treatment.

Finally, the thermal performance of a single test was reduced to the **module temperature range** which was calculated as the maximum temperature difference of any cell minus the minimum cell temperature difference of any other cell for the duration of the test. This gave the approximate overall maximum temperature difference experienced across the whole module for the whole test duration.

Reference Performance Tests

A summary of the capacity fade results achieved are shown in Figure 10 as a function of the equivalent number of full-charge cycles on an energy basis. The worst performing test were L1, A1 and A2 in that order, followed by similar results for L2, L3 and L4. The results were counter intuitive as the expectation was that the improved thermal treatment afforded by the immersion cooling would benefit cell aging. The symbols indicate the timing of the RPTs, which were repeated in some instances for the A2 test.

A summary of the internal resistance rise is shown in Figure 11 with a clear separation between the tests

FIGURE 10 Static capacity fade comparison.

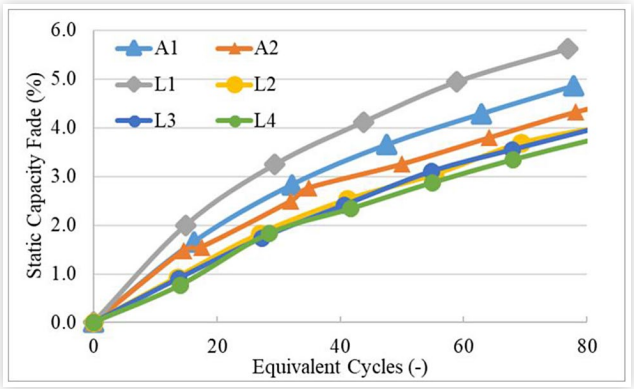

FIGURE 11 Resistance increase comparison.

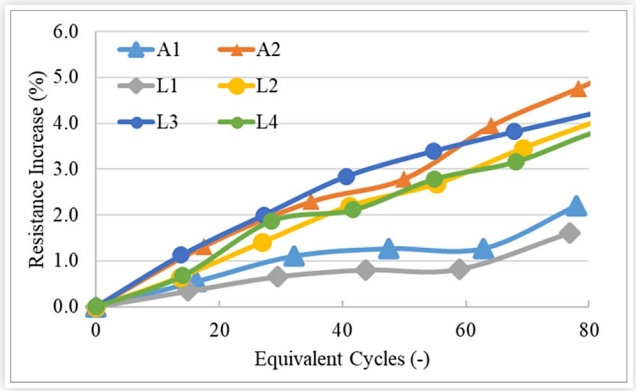

with poorly clustered cells (A1 and L1) that yielded distinctly lower resistance increases, and the better clustered cells (A2, L2, L3 and L4), regardless of thermal treatment.

Statistical Analyses

Due to the disparate results seen for the capacity fade for liquid immersion cooling compared to air cooling, further analyses were performed on the factors that were expected to influence cell aging. The response of the average module temperature, the standard deviation of the MD – indicating the electrical similarity- and the module temperature range – indicating the thermal homogeneity – was plotted against static capacity fade and shown in Figure 12. For this analysis, the capacity fade at the same terminal number of equivalent cycles was considered for all modules. Although there were general positive correlations for all variables, there was also much variability, for example the fact that the highest capacity did not exhibit a large module temperature range nor the highest test temperature.

Applying multiple linear regression to the data revealed a robust model with an adjusted R^2 value of more than 98% and p-values for all variables far below 0.05. The final model form was:

$$Fade = C1 + C2.MDstd + C3.Trange \quad (1)$$

FIGURE 12 Response of electric and thermal similarity to capacity fade.

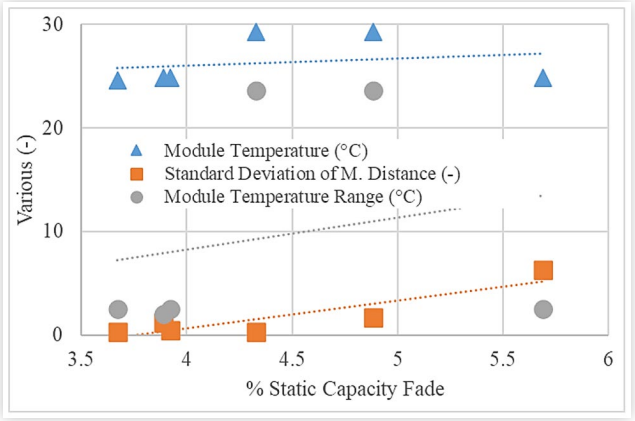

with C1, C2 and C3 empirically determined constants and all positive, with *MDstd* and *Trange* the standard deviation of the MD and the module temperature range, respectively. Test temperature and the average MD were also considered but either yielded counter-intuitive results (due to interaction with other variables) or were not significant in the model. The magnitude of C2 was about twice that of C3, meaning the fade was twice as sensitive to a unit change in the MD compared to a unit change in temperature. The values of these constants were such that a unit increase in the MD led to an 8% increase in capacity fade, whereas a 1 °C increase in the module temperature range caused a 4% change.

A similar analyses of the relation between resistance increase and operational data was explored but did not reveal any meaningful correlations beyond the earlier visual observations.

Discussion and Conclusions

This paper compared the aging of six different seven-cell modules. Each module was constructed from seven 21700 cylindrical cells that were provided with thermocouple measurements and arranged in a flower configuration.

The following observations were made:

- The characteristic of the cells in modules that were not intentionally clustered were widely distributed as seen by a bigger standard deviation of the MD, compared to cells that we clustered.
- MD was based on five cell characteristics, viz. discharge static capacity, charge and discharge time constants, open circuit voltage and internal resistance.
- Two different thermal treatments were applied: natural air convection and forced convection with a dielectric coolant.

- All modules were subject to the same multi-week aging profile that included the assessment of static capacity and resistance during a weekly RPT.
- Direct liquid immersion cooling resulted in much lower cell temperature differences during the charging part of the cycle when compared to air cooling: less than 2 °C for the former compared to more than 20 °C for the latter.
- This temperature increase showed an upward trend as the tests progressed, presumably due to increase in resistance and heat generated at a fixed current level.
- Both capacity fade and resistance increased during the four weeks of cycling, but the increases did not follow the module temperature ranges.
- The application of a statistical model revealed the capacity fade was positively correlated with both the electrical dissimilarities of the cells in a module (standard deviation of the MD) and the thermal dissimilarities (temperature range experienced by the module during the test). The former was approximately twice as sensitive to a unit change in the independent variable as the latter.
- The resistance increase for electrically dissimilar cells were lower than that of the clustered cells, regardless of the thermal treatment, but the exact reason for it is not known. It can only be speculated that balancing of the parallel connected cells during cycling or rest may have contributed.
- Although the properties of the liquids were not considered, their effects on achieving thermal homogeneity were apparent when considering the reduced cell temperature differences and module temperature ranges.
- The quantification of the impact of changes in single cell characteristics on module variability is not trivial and is a dynamic result of the cell population. For illustration purposes, using the data for the cells in this paper, a 10% increase in the discharge time constant of just one cell could increase the standard deviation of the MD by one.
- The paper clearly concluded that the cell selection and appropriate clustering of cells in a module is as important as thermal treatment and that the former can easily overshadow the latter, leading to possible incorrect conclusion about the efficacy of immersion cooling.

Recommendations

The following recommendations can be made after considering the results from this paper:

- Whereas the paper clearly showed the impact of electrical dissimilarities on the aging of cells connected and cycled in parallel, it did not address the reasons. This line of research is suggested for future work and may include the measurement of individual cell currents during both cycling and rest periods, during which time cell balancing is anticipated.
- The impact of further improvements in cell clustering for module construction, including the consideration of additional cell characteristics should be considered: The impact clustering may have on the variability that is observed during both aging and abuse tests should be investigated.
- The relative importance of the electrical property variability should be considered in relation to the absolute properties of the electrical properties. An intentional study of these variables is encouraged.
- This paper did not independently study the impact of test temperature which is known to affect aging. A structured investigation of both absolute cell temperatures, combined with temperature homogeneity should be attempted. This may be achieved by applying variations to the immersion cooling such as flow rates, geometry and fluids.
- Further improvements in the temperature homogeneity may be evaluated to see if aging outcomes can be further improved.
- The nature of the cell temperature difference over time and potential relation to the increase in module resistance should be investigated.
- Although this paper did not focus on the properties of the fluids used for direct liquid immersion cooling, an exploration of the fluid properties and their impact on heat transfer characteristics is warranted.
- This study was limited to nominal C-rates and did not explore the behavior at true fast-charge conditions. The robustness of the conclusions of this paper should be explored under more severe use conditions.

References

1. Mohammadian, S.K. and Zhang, Y., "Thermal Management Optimization of an Air-Cooled Li-Ion Battery Module using Pin-Fin Heat Sinks for Hybrid Electric Vehicles," *Journal of Power Sources* 273 (2015): 431-439, doi:10.1016/j.jpowsour.2014.09.110.
2. Lu, Z., Meng, X.Z., Wei, L.C., Hu, W.Y. et al., "Thermal Management of Densely-Packed EV Battery with Forced Air Cooling Strategies," *Energy Procedia* 88 (2016): 682-688, doi:10.1016/j.egypro.2016.06.098.
3. Akbarzadeh, M., Jaguemont, J., Kalogiannis, T., Karimi, D. et al., "A Novel Liquid Cooling Plate Concept for Thermal Management of Lithium-Ion Batteries in Electric Vehicles," *Energy Conversion and Management* 231 (2021): 113862, doi:10.1016/j.enconman.2021.113862.

4. Chung, Y. and Kim, M.S., "Thermal Analysis and Pack Level Design of Battery Thermal Management System with Liquid Cooling for Electric Vehicles," *Energy Conversion and Management* 196 (2019): 105-116, doi:10.1016/j.enconman.2019.05.083.
5. Javani, N., Dincer, I., Naterer, G.F., and Yilbas, B.S., "Heat Transfer and Thermal Management with PCMs in a Li-Ion Battery Cell for Electric Vehicles," *International Journal of Heat and Mass Transfer* 72 (2014): 690-703, doi:10.1016/j.ijheatmasstransfer.2013.12.076.
6. Yuan, X., Tang, A., Shan, C., Liu, Z. et al., "Experimental Investigation on Thermal Performance of a Battery Liquid Cooling Structure Coupled with Heat Pipe," *Journal of Energy Storage* 32 (2020): 101984, doi:10.1016/j.est.2020.101984.
7. Wu, S., Lao, L., Wu, L., Liu, L. et al., "Effect Analysis on Integration Efficiency and Safety Performance of a Battery Thermal Management System based on Direct Contact Liquid Cooling," *Applied Thermal Engineering* 201 (2022): 117788, doi:10.1016/j.applthermaleng.2021.117788.
8. Suresh Patil, M., Seo, J.-H., and Lee, M.-Y., "A Novel Dielectric Fluid Immersion Cooling Technology for Li-Ion Battery Thermal Management," *Energy Conversion and Management* 229 (2021): 113715, doi:10.1016/j.enconman.2020.113715.
9. Tan, X., Lyu, P., Fan, Y., Rao, J. et al., "Numerical Investigation of the Direct Liquid Cooling of a Fast-Charging Lithium-Ion Battery Pack in Hydrofluoroether," *Applied Thermal Engineering* 196 (2021): 117279, doi:10.1016/j.applthermaleng.2021.117279.
10. Wang, Y., Rao, Z., Liu, S., Li, X. et al., "Evaluating the Performance of Liquid Immersing Preheating System for Lithium-Ion Battery Pack," *Applied Thermal Engineering* 190 (2021): 116811, doi:10.1016/j.applthermaleng.2021.116811.
11. Williams, N.P., Trimble, D., and O'Shaughnessy, S.M., "An Experimental Investigation of Liquid Immersion Cooling of a Four Cell Lithium-Ion Battery Module," *Journal of Energy Storage* 86 (2024): 111289, doi:10.1016/j.est.2024.111289.
12. Gao, Q., "Performance Investigation of a Liquid Immersion Cooling System with Fish-Shaped Bionic Structure for Lithium-Ion Battery Pack," *International Journal of Heat and Mass Transfer* (2024).
13. Hemavathi, S., "Performance Evaluation of a Hydrostatic Flow Immersion Cooling System for High-Current Discharge Li-Ion Batteries," *Journal of Energy Storage* (2023).
14. Liu, J., "Comparative Study of Natural Ester Oil and Mineral Oil on the Applicability of the Immersion Cooling for a Battery Module," *Renewable Energy* (2024).
15. Li, C., Wang, Y., Sun, Z., Wen, X. et al., "Two-Phase Immersion Liquid Cooling System for 4680 Li-Ion Battery Thermal Management," *Journal of Energy Storage* 97 (2024): 112952, doi:10.1016/j.est.2024.112952.
16. Wang, Y., "Experimental Studies on Two-Phase Immersion Liquid Cooling for Li-Ion Battery Thermal Management," *Journal of Energy Storage* (2023).
17. Choi, H., Jun, Y., Chun, H., and Lee, H., "Comprehensive Feasibility Study on Metal Foam use in Single-Phase Immersion Cooling for Battery Thermal Management System," *Applied Energy* 375 (2024): 124083, doi:10.1016/j.apenergy.2024.124083.
18. Salvi, S.S., Surampudi, B., Swarts, A., Sarlashkar, J. et al., "Experimental and Theoretical Analysis of Immersion Cooling of a Li-Ion Battery Module," *Journal of Electrochemical Energy Conversion and Storage* 21, no. 4 (2024): 041001, doi:10.1115/1.4063914.
19. Feng, X., Zhang, X., and Xiang, Y., "An Inconsistency Assessment Method for Backup Battery Packs based on Time-Series Clustering," *Journal of Energy Storage* 31 (2020): 101666, doi:10.1016/j.est.2020.101666.
20. Yang, C., Wang, X., Fang, Q., Dai, H. et al., "An Online SOC and Capacity Estimation Method for Aged Lithium-Ion Battery Pack Considering Cell Inconsistency," *Journal of Energy Storage* 29 (2020): 101250, doi:10.1016/j.est.2020.101250.
21. Omariba, Z.B., Zhang, L., and Sun, D., "Review of Battery Cell Balancing Methodologies for Optimizing Battery Pack Performance in Electric Vehicles," *IEEE Access* 7 (2019): 129335-129352, doi:10.1109/ACCESS.2019.2940090.
22. Juarez-Robles, D., Azam, S., Jeevarajan, J.A., and Mukherjee, P.P., "Degradation-Safety Analytics in Lithium-Ion Cells and Modules Part II. Overcharge and External Short Circuit Scenarios," *J. Electrochem. Soc.* 168, no. 5 (2021): 050535, doi:10.1149/1945-7111/ac001f.
23. Nazari, M., Hussain, A., and Musilek, P., "Applications of Clustering Methods for Different Aspects of Electric Vehicles," *Electronics* 12, no. 4 (2023): 790, doi:10.3390/electronics12040790.
24. LG Chem, Product Specification: Rechargeable Lithium Ion Battery (Model: INR21700 M50 18.20Wh)., 2016.
25. Brereton, R.G., "The Mahalanobis Distance and its Relationship to Principal Component Scores," *Journal of Chemometrics* 29, no. 3 (2015): 143-145, doi:10.1002/cem.2692.

Contact Information

The authors can be contacted at:
andre.swarts@swri.org

Acknowledgments

The authors wish to acknowledge support of the members of the SwRI Electric Vehicle and Energy Storage Evaluations (EVESE) consortium.

Definitions/Abbreviations

BOL - Beginning of life
CC - Constant current
CCCV - Constant current constant voltage
LIB - Lithium-ion batteries
MD - Mahalanobis distance
NMC - Nickel manganese cobalt oxide
OCV - Open circuit voltage
PCM - Phase change materials
RPT - Reference performance test
SEI - Solid electrolyte interphase
SOC - State of charge

ISSN 0148-7191